RESEARCH ARTICLE | JUNE 02 2025

Power law distribution and multi-scale analysis in Earth sciences, finance, and other fields: Some guidelines to parameter estimation

Vincenzo Guerriero ; Marco Tallini

Chaos 35, 063102 (2025)
https://doi.org/10.1063/5.0259215

Power law distribution and multi-scale analysis in Earth sciences, finance, and other fields: Some guidelines to parameter estimation

Cite as: Chaos 35, 063102 (2025); doi: 10.1063/5.0259215
Submitted: 18 January 2025 · Accepted: 12 May 2025 ·
Published Online: 2 June 2025

Vincenzo Guerriero[a] and Marco Tallini

AFFILIATIONS

Department of Civil, Construction-Architectural and Environmental Engineering, University of L'Aquila, L'Aquila 67100, Italy

[a]**Author to whom correspondence should be addressed:** vincenzo.guerriero@univaq.it

ABSTRACT

Power-law distributions, with their interdisciplinary applications in fractals, non-linear systems, chaos theory, self-organized criticality, and scale-free systems, have garnered significant attention in recent decades. These theories find applications across various scientific disciplines, from physics to Earth sciences, social sciences, economics, and finance. Parameter estimation for such distributions can be effectively conducted by examining data at multiple scales of observation. This article illustrates practical multi-scale analysis methods through case studies from the statistical analysis of rock fractures and financial data, explaining their advantages and the underlying hypotheses and theories. Furthermore, a novel version of a maximum likelihood-based parameter estimation criterion, adapted for multi-scale samples, is presented, reassuring the audience about its applicability.

How can we estimate the probability that the Euro–U.S. dollar exchange rate will fluctuate by more than 1% in the next hour or that an earthquake greater than five on the Richter scale will impact our homes within the next year? To address these questions, we must first recognize that the time series of these quantities, measured moment by moment, follow statistical distributions distinct from the familiar ones where the variable studied shows an expected value and a specific degree of variability (e.g., Normal, Log-Normal, etc.). These quantities are distributed according to a power law. This statistical distribution is characterized by exceptional (or catastrophic) events occurring significantly more frequently than anticipated. It is typically associated with phenomena observed in many chaotic, complex, or scale-free systems. It is present across a wide range of scientific disciplines. Parameter estimation, particularly of the power-law exponent, can be effectively performed by observing the variable in question over multiple orders of magnitude or through a multi-scale analysis. In this article, we outline two alternative multi-scale statistical methods for estimating the exponent, one of which is new (based on a maximum likelihood criterion), while the other is relatively recent. We illustrate the potential application areas for these methods and compare them, clarifying when one method may be preferred over the other. No previous studies have directly compared the methods discussed, comprehensively analyzing their underlying assumptions and performance. The examined techniques have broad applicability across various scientific fields.

I. INTRODUCTION

Consider the market value of cars passing through a toll booth or a specific road section in a certain timeframe, and assume that for each vehicle, the probability $P(x)$ of value exceeding x is

$$P(x) = Cx^{-m}, \tag{1}$$

where C and m are the positive constant parameters and x is a positive real number.

We now have an attribute (car value), distributed according to a power law, which is associated with an event (road section crossing) whose time distribution may be known (often assumed to be a Poisson distribution). A time series of cumulative cars' market values passing per time unit, e.g., seconds (i.e., for a single car), or hours, or days, can be associated with these observations. This example

goes beyond mere curiosity when considering that the total economic value of damage (and corresponding compensation) to cars involved in road accidents within a given area may exhibit a similar probability distribution. Knowledge of such a distribution enables insurance companies to conduct essential risk analyses, allowing them to remain economically viable and policyholders to receive due compensation.

In finance, the value of buy/sell orders for several stocks or other derivatives, arriving at a bank over time, exhibits a power-law distribution,[1] where the distribution over time is particularly sensitive to market hours, news, macroeconomic or geopolitical events, etc. Note that the distribution in Eq. (1) is the complementary probability distribution function of a variable X, defined as $P(x) = \text{Probability}(X \geq x)$. To streamline the exposition, in the following text, we will refer to the probability $P(x)$ simply as the distribution. Furthermore, as X is here described by a real number, Eq. (1) denotes a continuous power-law distribution. The related probability density function (pdf) also follows a power law.

Power-law distribution appears in several scientific fields such as physics, Earth science, ecology, economics and finance, computer science, demography, and social sciences (e.g., Refs. 2–17 and references therein). Several quantities show such a statistical distribution, e.g., price movements in financial markets, earthquake size, and city population. In the last decades, power-law distribution is raising an increasing interest as, in fields such as the theory of fractals, of nonlinear systems, chaos theory, self-organized criticality, and scale-free networks, it plays a key role.

Power-law distributions are characterized by a greater frequency of small values compared to larger ones. Additionally, they appear as a straight line on a log–log plot, regardless of the scale of observation. This scale-free property is a defining characteristic of power-law distributions.

Figure 1 presents a time series of the Euro–US dollar exchange rate (real-world data) and the empirical distribution of the absolute difference between closing and opening prices within a minute, spanning 1 January 2015 to 30 June 2017. Beyond the threshold of about 0.0003–0.0005, the blue dots align well with a power-law trendline. Below this threshold (light red dots), the values follow a different distribution.

Note that in Fig. 1, plot on the right, the y axis displays the probability $P(x)$ [Eq. (1)] on the left and the cumulative frequency on the right. The cumulative frequency, defined as the number of events per unit time (in this case, per month) exceeding x, provides useful information about data. It indicates the monthly frequency of price swings exceeding a certain threshold or reaching certain extreme values, which is a fundamental information in financial risk evaluation. It is recalled here that the occurrence probability of rare extreme events (possibly leading to financial crashes) showing power-law distribution may be of several orders of magnitude greater than that associated with other usual models (e.g., exponential, Fig. 1; Refs. 1 and 10).

Other relevant examples of this kind of distribution in geophysics and Earth sciences include seismic events and fractures/faults at various scales. According to the Gutenberg–Richter law, earthquake size (expressed as associated fault area or peak ground acceleration) follows a power-law distribution.[14,16,17] On a smaller scale, tensional fractures in rocks (i.e., joints) also exhibit such distribution. These joints usually occur in parallel sets, with their opening displacements (apertures) frequently following a power-law distribution, ranging from the outcrop scale to the crystal scale.[18–22] Additionally, considering a given sampling line perpendicular to fracture planes (scanline), these fractures are often randomly distributed along the line (i.e., these show a spatial Poisson distribution[20,23,24]).

Figure 2(a) shows the cumulative frequency of tensile fracture aperture measured, at Faito Mt. (Naples, Italy), along two scanlines at different scales: (i) a field scanline 3 m long, measured with the naked eye or a hand lens and (ii) a micro-scanline 1.9 cm long,

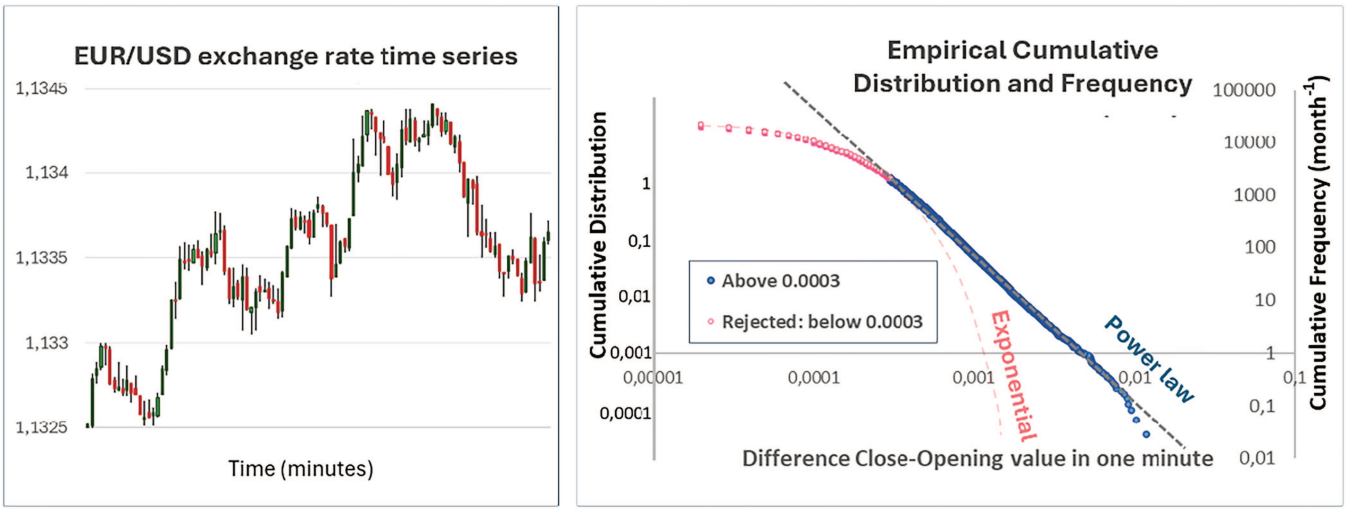

FIG. 1. Time series of the exchange rate of Euro vs US dollar (real data) and cumulative distribution and frequency of the price swing, described as the absolute value of difference between close and opening values within a minute, along the time range from 1 January 2015 to 30 June 2017 (sample of 931.243 data).

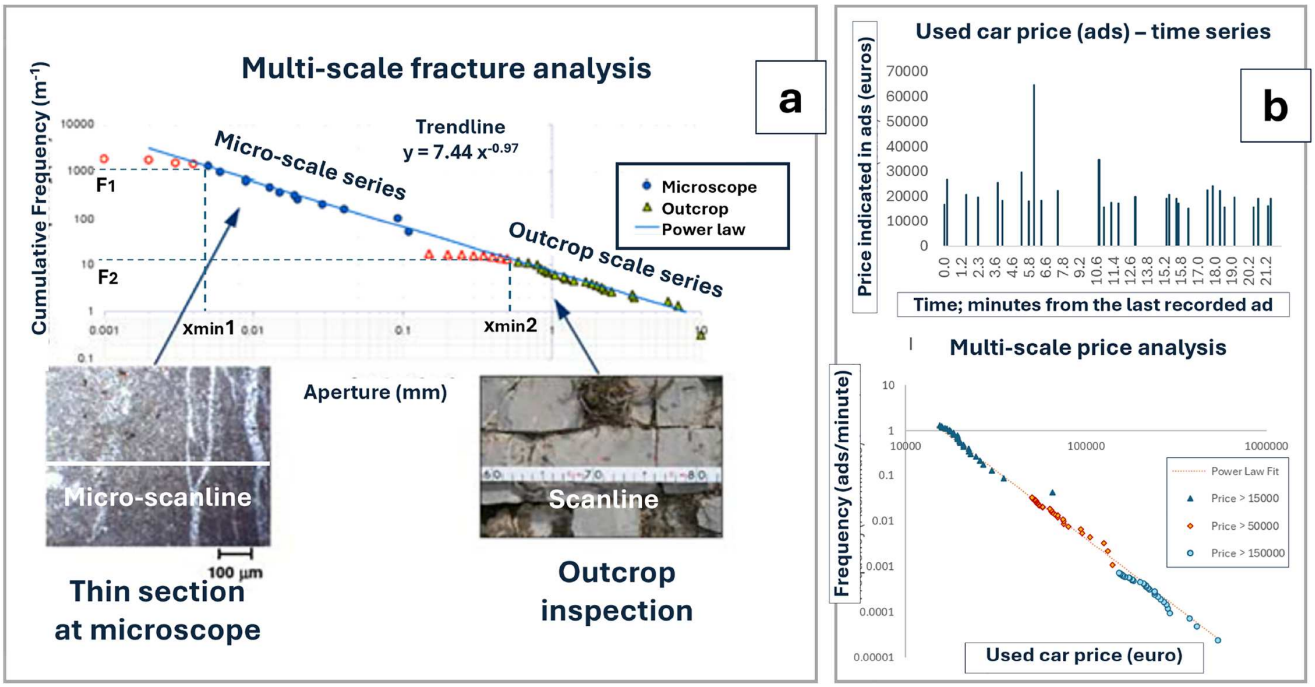

FIG. 2. Examples of multi-scale statistical analysis. (a) Distribution of tensile fracture aperture values, observed at the meter scale on outcrop with naked-eye measurements, and at the micro-scale, with measurements taken under a microscope on a thin section of rock. Red dots denote the frequency values underestimated due to the low visibility of smaller fractures at that scale (i.e., truncation artifact; Ortega *et al.*[18]). (b) Distribution of proposed prices for used cars on an online marketplace, observed at three different scales. The time series shown at the top refers to the sample of listings with prices exceeding €15 000 (dark blue points in the down plot).

measured by microscope on thin section of rock. Details about the sampling techniques and the study area can be found in the paper by Guerriero *et al.*[20,21] Due to the challenges associated with measuring the aperture of small fractures, which are often poorly visible, multi-scale analyses are commonly employed.[18–22]

In this study, the multi-scale analysis refers to a statistical investigation conducted across multiple scales of observation using appropriate instruments or sampling criteria. This approach allows for the examination of the cumulative frequency of the observed variable over several orders of magnitude. For instance, in the analysis of fracture aperture, one sample of values is collected in field (by naked eye or using a hand lens) and a second sample is obtained using an optical microscope on a thin section, enabling the observation of a significant number of fractures with apertures ranging from a few micrometers to several millimeters. To illustrate this approach, we compare multi-scale analyses of fractures with examples from finance and economics.

Figure 2(b) illustrates the cumulative frequency of used car advertisements with price (pr) exceeding 15 000 euros on a popular Italian classified website. The ordinate represents the number of ads posted per minute with prices greater than or equal to the abscissa value. Sampling has been conducted according to a multi-scale approach, based on three sub-samples of 30 elements each. The first sub-sample was achieved by recording the timestamp of the last 30 ads for which $pr \geq 15\,000$ euros, the second sub-sample considering $pr \geq 50\,000$ euros, and the third considering $pr \geq 150\,000$ euros. Prices below the 15 000 euros threshold were not analyzed due to their apparent deviation from power-law distribution. For used car prices, what allows a multi-scale approach is the sampling criterion; three samples, each consisting of 30 values, are collected considering three different price thresholds (15 000, 50 000, and 150 000 euros). This allows for the observation of prices ranging from 15 000 to several hundred thousand euros using a sample of only 90 listings.

The cumulative frequency $F(x)$ of a property X (in this case, price) provides a convenient alternative to the cumulative distribution function. A variable exhibiting power-law cumulative frequency with exponent m also follows a power-law distribution function with the same exponent but a different coefficient (Fig. 1). Cumulative frequency offers advantages, such as allowing data from different time (or length) windows to be plotted on the same diagram (Fig. 2), so enabling us to conduct a multi-scale analysis. This is particularly useful when the temporal (or spatial) distribution of the events is known.

It is generally assumed that the power-law distribution holds for values above a minimum threshold, $x_{\min}$, where $P(x_{\min}) = 1$. According to Eq. (1), this condition leads to

$$C = {x_{\min}}^{m}. \tag{2}$$

In some cases, $x_{\min}$ represents the point below which the distribution deviates from the power law, as observed in the examples

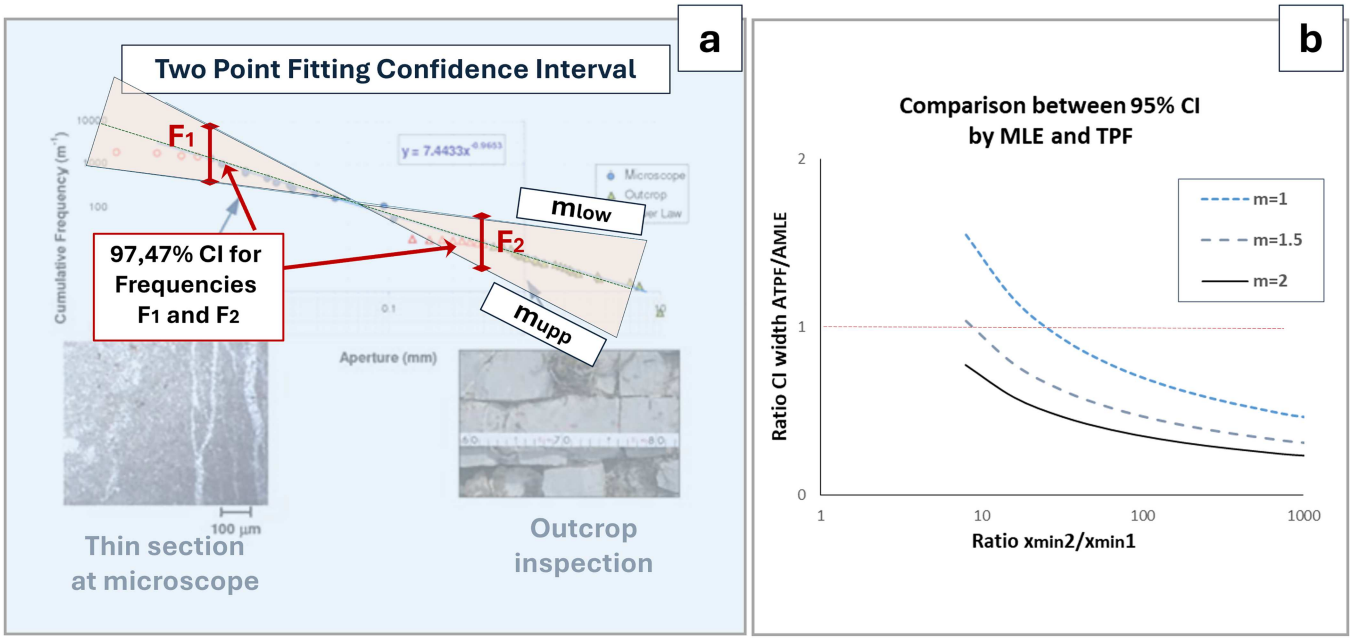

FIG. 3. (a) 95% confidence interval for trendline slope. The confidence intervals of frequencies *F*1 and *F*2 (dark red vertical segments) are not in scale to improve the image readability. The values m_{upp} and m_{low} denote, respectively, the maximum and minimum trendline slope, under the hypothesis that this line is contained within each one of the two frequency confidence intervals. (b) Comparison between the width of confidence intervals estimated by the MLE and TPF approaches for a varying ratio $x_{min}2/x_{min}1$ and different exponent values. Where the ratio A_{TPF}/A_{MLE} is less than 1, TPF provides more accurate estimates than MLE (see the main text).

of the exchange rate and of car value [Figs. 1 and 2(b)]. In other cases, it is established conventionally to exclude small values that, although actually following power-law distribution, are affected by under-sampling [this bias is called truncation artifacts; Fig. 1(a); Refs. 18–20]. Value *C* can be viewed as unimportant normalizing constants. The key parameter characterizing power-law distributions is the exponent m. Nevertheless, the choice of x_{min} can be critical since this value can influence, in some cases significantly, the estimate of *m*. Useful methods for identifying the optimal value of x_{min} for a sample are illustrated by Clauset *et al.*[16] and by Barò and Vives.[25]

Power-law cumulative frequency and distribution generally lack finite mean and variance, making the central limit theorem inapplicable. Analyzing empirical data involves two primary goals: (i) verifying that the data are actually distributed according to a power law and (ii) estimating the parameter m.

While a detailed examination of the distribution verification is beyond the scope of this short communication, this topic will be briefly reviewed, with appropriate references provided for further reading. Regarding parameter estimation, the most effective criteria proposed in the literature are based on maximum likelihood estimation (MLE)[16,17,25–29] and, for multi-scale sampling, on two-point interpolation.[20]

The main aim of this short communication is to illustrate and compare these two alternative methods for parameter estimation in the multi-scale analysis of power-law distributions.

II. IDENTIFYING POWER-LAW DISTRIBUTION

In some cases, the distribution type may be a priori known based on the data's nature,[17] allowing direct estimation of the exponent without prior verification. Otherwise, a visual inspection of the empirical cumulative distribution (or frequency) on a log–log plot can be used. Empirical distribution can be timely achieved by means of the rank-frequency method (see Ref. 17 for distribution and Ref. 18 for cumulative frequency). However, this method requires a sufficiently large data set for reliability and may introduce potential biases.[16,17,26,27]

Given the availability of big data, recognizing power-law distributions in fields like social network interactions or financial data are often straightforward (Fig. 1 is based on nearly 1×10^6 real-world data, freely available). However, data collection can be costly in many other cases. Multi-scale analysis can effectively identify power-law distributions and estimate the exponent, even by means of relatively small samples of less than one hundred data points. This significantly reduces the costs associated with statistical sampling or investigation time, while maintaining satisfactory accuracy. By way of example, Fig. 2(b) is constructed using a sample of approximately 90 data points. Notably, only two of the three samples ($pr > 15\,000$ and $pr > 150\,000$) would have been sufficient to reasonably verify the alignment of data points across multiple price orders of magnitude. To observe the distribution of the same population over the same value range (from 15 000 to 539 000 euros) using a single-scale

sampling approach would have required sampling the observed values within the largest temporal window (24 days) using the smallest scale threshold (i.e., 15 000 euros), resulting in a sample size of over 46 000 values (Sec. III D).

Multi-scale empirical frequency distribution plots enable us to assess whether data series collected at different scales align with a common trendline [linear on a log–log plot; Figs. 1(a) and 1(b)] or exhibit distinct patterns. If the trendlines align, we can infer that the underlying populations share the same power-law distribution.

While this approach, albeit less rigorous, provides a practical tool in many experimental settings where data are expected to follow a power-law distribution and confirmation is sought, more rigorous methods have been proposed based on goodness-of-fit tests.[16,28–30] Some of these methods[16,28–30] rely on the integrated use of a Kolmogorov–Smirnov statistic, MLE, and Monte Carlo simulations. The underlying principle is as follows. The null hypothesis that the observed empirical distribution is drawn from a theoretical power-law model is tested by evaluating the "distance" between the two distributions using the simple Kolmogorov–Smirnov statistic (KSS). This is defined as the maximum absolute difference between the empirical and theoretical cumulative distributions. The theoretical distribution is determined using MLE. Denoting the observed value for the given sample by KSS*, the p-value is then calculated via Monte Carlo simulations, as a closed-form expression is not available. Therefore, starting from the estimated theoretical distribution, the following procedure is repeated a large number of times (several thousands): a simulated sample is generated, the theoretical distribution is estimated using MLE, and the KSS is calculated. The p-value is simply calculated as the percentage or fraction of KSS values obtained from simulations for which KSS > KSS*. The obtained p-value is compared to a chosen significance level to accept or reject the null hypothesis. Navas-Portella *et al.*[28] proposed a version of this method applicable to aggregated datasets, which may be suitably adapted to the case of multi-scale samples.

III. MULTI-SCALE STATISTICAL ANALYSIS IN PARAMETER ESTIMATION

Multi-scale exponent estimation can be conducted using two alternative methods: (1) a MLE-based formula if the distribution of events/values over time (or space) is not known and (2) a Two-Point Fitting (TPF) approach,[20] which offers advantages over MLE, but requires prior knowledge of temporal (or spatial) event distribution.

A. Maximum likelihood-based method

For the MLE approach, given two samples with N_1 and N_2 values and corresponding minimum thresholds $x_{\min}1$ and $x_{\min}2$, the exponent m can be estimated as follows (Appendix A):

$$m = (N1 + N2) \cdot \left(\sum_{j=1}^{N1} \ln \frac{x_j}{x_{\min}1} + \sum_{j=1}^{N2} \ln \frac{x_j}{x_{\min}2} \right)^{-1}, \quad (3)$$

where x_j denotes the measured values and $x_{\min}1$ and $x_{\min}2$ represent the minimum thresholds (not the smallest measured values). In rock fracture analysis, these thresholds are determined based on factors such as visibility and microscope quality. For instance, in Fig. 2(a),[20,21] $x_{\min}1$ and $x_{\min}2$ were set to 0.005 and 0.5 mm, respectively. This formulation is an adaptation of the criterion proposed by Navas-Portella *et al.*[28] (see also Ref. 17) to the case of multi-scale samples (Appendix A).

The expected error, σ, can be estimated as (Ref. 17; Appendix A)

$$\sigma = \frac{m}{\sqrt{N1 + N2 + 1}}. \quad (4)$$

These formulations can be readily extended to three or more samples [e.g., Fig. 2(b)] as follows. Given M samples, each including Nk values and with minimum thresholds $x_{\min}k$, Eqs. (3) and (4) become (Appendix A)

$$m = \left(\sum_{k=1}^{M} Nk \right) \cdot \left(\sum_{k=1}^{M} \sum_{j=1}^{Nk} \ln \frac{x_j}{x_{\min}k} \right)^{-1}, \quad (5)$$

$$\sigma = \frac{m}{\sqrt{1 + \sum_{k=1}^{M} Nk}}. \quad (6)$$

These estimators provide significantly more accurate results than the commonly used least squares method. Moreover, they do not require knowledge of the underlying spatial or temporal event distribution, unlike the TPF method discussed subsequently.

B. Two-point fitting approach

The TPF method[20] offers a straightforward approach to exponent estimation. While less commonly used, it provides significant advantages over both least squares and MLE [Eqs. (3)–(6)]. The method involves fitting a trendline through only two points: those corresponding to $x_{\min}1$ and $x_{\min}2$ [e.g., the boundary between red and blue points in the microscale series, or red and green in the outcrop series of Fig. 2(a)]. These points are selected based on the same criteria used for Eq. (2). Unlike Eq. (3), here $x_{\min}1$ and $x_{\min}2$ represent the smallest observed values for each series. The exponent is then calculated as the slope of the line connecting these two points on a log–log plot. Denoting by F_1 and F_2, the measured cumulative frequencies associated with $x_{\min}1$ and $x_{\min}2$ [Fig. 1(a)], respectively, the exponent m is estimated as[20]

$$m = -\frac{\ln\left(\frac{F_1}{F_2}\right)}{\ln\left(\frac{x_1}{x_2}\right)}. \quad (7)$$

The confidence interval (CI) for the exponent is determined by considering the cumulative frequency values F_1 and F_2 as estimates of expected values for random variables with their own CIs, whose limits can be denoted here by $F_{\text{upp}}1$, $F_{\text{low}}1$ and $F_{\text{upp}}2$, $F_{\text{low}}2$, respectively [Fig. 3(a); Ref. 20]. Denoting by y the probability that a trendline passes within one of CIs, then the probability of line passing through points within both CIs simultaneously is y^2. This latter is equal to the probability that $m_{\text{low}} < m < m_{\text{upp}}$, where m_{low} denotes the slope of the line for ($F_{\text{low}}1$, $x_{\min}1$) and ($F_{\text{upp}}2$, $x_{\min}2$), and m_{upp} that of the line for ($F_{\text{upp}}1$, $x_{\min}1$) and ($F_{\text{low}}2$, $x_{\min}2$) [Fig. 3(a)]. Clearly, m_{low} and m_{upp} can be viewed as the (y^2)% CI for m. Therefore, to calculate the 95% CI of m, we need to estimate the 97.47%

CIs for $F1$ and $F2$ (as $0.9747^2 = 0.95$). The 97.47% CIs for several values of the Poisson variable are illustrated in Appendix B (Table I). Therefore, the 95% CI for m is estimated as follows:

$$m_{\text{upp}} = -\frac{\ln\left(\frac{F_{\text{upp}}1}{F_{\text{low}}2}\right)}{\ln\left(\frac{x_1}{x_2}\right)}, \tag{8}$$

$$m_{\text{low}} = -\frac{\ln\left(\frac{F_{\text{low}}1}{F_{\text{upp}}2}\right)}{\ln\left(\frac{x_1}{x_2}\right)}. \tag{9}$$

A significant advantage of the TPF method is that it only requires counting events above the specified thresholds, significantly reducing data acquisition time. For example, in fracture analysis, only joints with apertures greater than or equal to $x_{\min}$ need to be counted (and not accurately measured) for each series. Once a preliminary analysis verifies that the spatial distribution is Poisson and the aperture distribution follows a power law in a certain area,[19–21] the subsequent analyses using TPF can be conducted without verifying distributions (and constructing plots), allowing for rapid estimation of the power-law exponent and its 95% CI.

The TPF method necessitates a known and constant temporal or spatial distribution of events. For instance, the TPF approach is inapplicable to Euro–US dollar exchange rates (Fig. 1) due to the highly variable temporal distribution of fluctuations influenced by economic news. For example, while the expected frequency of minute-by-minute fluctuations greater than or equal to 0.002 is approximately 11 times per month, based on the distribution in Fig. 1, the day after the Brexit referendum (24 June 2016) alone recorded 19 such fluctuations, equivalent to 570 occurrences per month. This significantly higher cumulative frequency, based on a small sample, would yield a drastically altered exponent estimate when calculated as the slope of the TPF line, rendering the method unreliable. Although the TPF approach is unsuitable for such data due to the availability of large freely accessible data sets, this simple example highlights how substantial variations in the temporal (or spatial) distribution of events can undermine the TPF estimation.

C. Pros and cons of TPF approach against MLE: A comparison

A comparison between MLE and TPF approaches can be made by comparing the widths of the 95% CIs obtained using both methods. Geometric considerations show that the TPF CI narrows as the ratio $x_{\min}2/x_{\min}1$ increases. Figure 3(b) shows the ratio of the 95% CI widths for TPF and MLE as a function of $x_{\min}2/x_{\min}1$ for three exponent values m in the range 1–2 (commonly observed values[16]). The width of the MLE 95% CI is denoted by $A_{\text{MLE}} = 2\sigma$ [Eq. (4)], while that of the TPF 95% CI by $A_{\text{TPF}} = m_{\text{upp}} - m_{\text{low}}$ [Eqs. (8) and (9)]. Figure 3(b) highlights that for large values of the ratio $x_{\min}2/x_{\min}1$ (e.g., >100), TPF consistently provides more accurate estimates than MLE (as $A_{\text{TPF}}/A_{\text{MLE}} < 1$). For smaller values of this ratio, the accuracy of the TPF estimate relative to MLE depends on the exponent value. The optimal choice is to use the TPF criterion if the ratio $A_{\text{TPF}}/A_{\text{MLE}}$ is significantly less than 1. If, however, this ratio is close to 1, the choice should be carefully evaluated, as the MLE estimate of m [Eqs. (6)–(9)] has the advantage of not requiring assumptions about the temporal or spatial distribution of the observed events, while the TPF estimate offers significantly faster data acquisition.

D. A practical example of estimation

We now estimate the exponent m for rock fracture aperture data using both methods. The sample consists of 24 values greater than or equal to 0.005 mm from a 19 mm thin section micro-scanline and 41 values greater than or equal to 0.5 mm from a 3 m outcrop scanline. The MLE method [Eq. (3)] yields $m = 1.13$ with an expected error of $\sigma = \frac{1.13}{\sqrt{24+41+1}} = 0.14$. The 95% CI is estimated as $m = 1.13 \pm 1.96 \cdot 0.14 = 1.13 \pm 0.27$.

TPF is simpler. Given the sample sizes, the frequencies (i.e., joints per meter) are $F1 = 1263\ \text{m}^{-1}$ and $F2 = 13.67\ \text{m}^{-1}$. Assuming a Poisson distribution,[19–21,24] the 97.47% CIs are (m^{-1}): $F_{\text{upp}}1 = 1974$, $F_{\text{low}}1 = 798$, $F_{\text{upp}}2 = 19.3$, and $F_{\text{low}}2 = 9.61$. Equation (7) yields $m = -\frac{\ln\left(\frac{1260}{13.67}\right)}{\ln\left(\frac{0.005}{0.5}\right)} = 0.98$, and Eqs. (8) and (9) yield the 95% CI limits: $m_{\text{upp}} = -\frac{\ln\left(\frac{1964}{9.64}\right)}{\ln\left(\frac{0.005}{0.5}\right)} = 1.16$ and $m_{\text{low}} = -\frac{\ln\left(\frac{797}{19.20}\right)}{\ln\left(\frac{0.005}{0.5}\right)} = 0.81$. The 95% CI widths are 0.55 for MLE and 0.35 for TPF, showing TPF's greater accuracy. Furthermore, it is recalled that TPF only requires counting values above the threshold, while MLE requires measuring all values.

For online used car prices, with two series of 30 values each: the small-scale series include ads, with prices > 15 000 euros, recorded within 22 min, and the other series include ads with price > 150 000 euros, recorded within 34 560 min (ca. 24 days).

MLE gives the following estimate for m 95% CI: $m = 2.81 \pm 0.70$. TPF yields $m = 3.21$, $m_{\text{upp}} = 3.57$, and $m_{\text{low}} = 2.86$. Again, the TPF CI width (0.71) is significantly narrower than that of MLE CI (1.41). On the other hand, short-term recordings may be affected by temporal variations, as frequencies (published ads per minute) can change by time of day or day of the week. In the case study here illustrated, preliminary analysis suggests that frequencies recorded on weekday afternoons are similar to long-term averages, justifying the use of TPF. In general, TPF should be used cautiously when temporal variations are present. Finally, we emphasize that to observe the distribution of car prices on the same range of values examined here, which goes from 15 000 euros to the maximum recorded value of 539 000 euros, through a traditional single-scale sampling, it would have been necessary to sample all the ads with a price greater than 15 000 euros published in 24 days for a total of approximately 46 600 values.

IV. INTERPRETING POWER-LAW DISTRIBUTIONS IN INFERENTIAL ANALYSIS

The results of inferential analysis necessitate careful interpretation alongside a thorough evaluation of their associated uncertainties. Parametric inferential analysis operates under the assumption that the probability distribution of the observed quantity is known. Within this framework, key uncertainties can arise from overfitting, the width of a parameter estimate's confidence interval [Ref. 31 (pp. 341–371) and Ref. 32 (pp. 90–96 and 119–148)] and the correctness of the assumed probability distribution model. Here, overfitting

is not a primary concern, as it typically emerges when estimating too many parameters from a limited sample size [Ref. 32 (p. 218) and Ref. 33 (pp. 298–300)]; our methods focus on estimating a single parameter, the exponent. The use of confidence intervals to describe the uncertainty associated with parameter estimation is a well-established method [Ref. 32 (pp. 90–96) and Ref. 31 (pp. 341–371)]. A more subtle challenge can stem from the application of inappropriate statistical models for inferential analysis or the adoption of incorrect underlying assumptions. Making such assumptions generally requires justification also based on external information about the population being analyzed.

For instance, in seismological studies, seismic hazard assessment is grounded in a comprehensive understanding of the geological and seismotectonic setting of the study area, including the identification of major active faults and seismogenic zones.[34] Furthermore, nearly a century of seismographic data confirm that magnitudes such as fault area or peak ground acceleration associated with seismic events are distributed according to a power law. Statistical analysis of seismic event records in a specific area complements these analyses by providing quantitative data on the probability distribution of magnitude values (the Gutenberg–Richter law). It should be noted that, due to considerable uncertainties in geological and geophysical data, multiple interpretations of models are often possible, and one of the problems of probabilistic seismic hazard analysis is the comparison and choice between multiple models.[34]

The prevalence of power-law distributions in numerous phenomena, including, e.g., earthquakes, forest fires, and financial crashes, is often explained through the lens of self-organized criticality,[12–14] a model that proves that the size of quantities such as fault area, the number of trees involved in a fire, or price fluctuations in financial markets follow a power law. Additional mechanisms generating quantities with power-law distributions are detailed by Newman[17] and other authors.[16,35,36] In a previous study, Zamankhan *et al.*[35] utilized wavelet analysis as a method to conduct a scale analysis involving chaotic systems exhibiting fractal-like structures.

As the two described methods, TPF and MLE, are parametric, it is essential that their underlying assumptions are supported by a known theoretical model or by other statistical investigations, such as goodness-of-fit tests (Sec. II). For example, as highlighted in Sec. III B, the TPF method is inadequate to apply to financial data due to the temporal variability of market trading, which violates the assumption of a constant Poisson temporal distribution, leading to a biased exponent estimate (Sec. III B). When aiming to analyze stock or currency prices across multiple time scales (e.g., daily and multi-year[1]), it is crucial to recognize the limitations of the TPF method and to design statistical investigations that account for market conditions significantly influencing quotations. Furthermore, the temporal constancy of the distribution should generally also be verified. For instance, Mandelbrot and Hudson[1] illustrated a study comparing daily fluctuations in cotton prices across two distinct time periods, as well as comparing daily with monthly oscillations. The finding that these three distributions exhibited a power law with the same exponent suggested an inherent characteristic of the global cotton market, irrespective of the temporal scale or epoch considered. However, fully capturing the human behavior's complexities within financial markets presents a significant challenge. When considering extreme economic events linked to unexpected news (by way of example, as the 2016 Brexit outcome, the same year's US presidential election, or the recent market turbulence associated with US presidential decisions in April 2025), one might hypothesize that extreme price variations in stocks or indices are encompassed within a long-term statistical distribution, similar to the cotton prices studied by Mandelbrot. Nevertheless, this assumption requires confirmation. The alternative hypothesis, that new technological advancements or shifts in market dynamics could alter the statistical distributions of current price oscillations compared to the past, cannot be rejected without evidence. Consequently, any analysis of these oscillations should be preceded by a verification that price fluctuations recorded across different scales or time intervals follow the same underlying distribution, e.g., using the methods outlined in Sec. II.[28–30]

Regarding the potential application of the illustrated inferential methods for forecasting, it is worth noting that extreme events associated with complex phenomena, such as destructive earthquakes or economic crashes, are considered inherently unpredictable. According to the self-organized criticality model,[13,14] these events exhibit intensities distributed according to a power law, and extreme occurrences are considered fundamentally unpredictable in the sense that we cannot know, for example, whether the next price fluctuation of the Euro–US dollar exchange rate or the next earthquake will be moderate or extreme. However, an appropriate inferential analysis of the power-law distribution allows for long-term probabilistic forecasts of extreme events. On the other hand, short-term forecasting requires different approaches and technological advancements and data analysis could lead to more accurate short-term predictions, thus undermining the argument for relying solely on long-term probabilistic forecasts.

For instance, in seismic hazard assessment, a well-established procedure (aimed at the seismic design of structures) calculates, based on the magnitude distribution law, the probability that an earthquake with a ground acceleration exceeding a certain threshold will occur at a given site within timeframes ranging from decades to centuries.[34] Note that risk analysis in seismology,[34] as well as in other fields, operates on the premise of accepting a tolerable probability that an extreme event will exceed a certain threshold. When such an exceedance occurs, damage to individuals or organizations affected by the adverse extreme event is unavoidable. Consequently, this limiting probability is established at a level deemed reasonably "small."

Similarly, in finance, knowledge of the power-law distribution of price fluctuations, while not enabling short-term predictions, allows for risk analysis. When placing a buy or sell order for a financial product or derivative, we cannot know whether the price variation will be favorable or not. However, by knowing the power-law distribution of price fluctuations (in absolute value), we can estimate the probability that our loss may exceed a certain threshold within a specific timeframe (daily, weekly, annually, etc.[1]).

V. CONCLUSIONS

Multi-scale analysis offers significant advantages over traditional approaches when studying quantities exhibiting power-law distribution, facilitating parameter estimation. Empirical cumulative frequency plots obtained from two or more samples, gathered

at different scales [Figs. 2(a) and 2(b)], allow to identify data point alignment with power-law distributions across multiple orders of magnitude of the studied variable.

The power-law exponent can be effectively estimated from a multi-scale sample using two alternative methods: (i) maximum likelihood estimation (MLE) and (ii) two-point fitting (TPF) approach. Here, we propose a version of the MLE-based estimation criterion, adapted to the case of multi-scale samples, which can be applied to two or more samples at different scales and does not require assumptions about the temporal or spatial distribution of measured events. TPF offers the advantage of more accurate estimation and significantly faster sampling (requiring only counting values above a threshold, not precise measurement), but is limited to pairs of samples at different scales and requires a known and constant temporal or spatial distribution of the measured events.

ACKNOWLEDGMENTS

The author thanks the Editor and Reviewers for their constructive comments and suggestions, which helped to significantly improve this manuscript. The research leading to these results has received funding from the Italian Ministero dello Sviluppo Economico (MiSE) under the project "SICURA—Casa Intelligente delle Tecnologie per la Sicurezza", Grant Id: C19C20000520004, from the University of L'Aquila, under the project with Grant Id: 03AT2025GUEPAR, and from the ArtEmis Project funded by the European Union, under Grant Id: 101061712. The research described in this paper has been developed in the framework of the research project National Centre for HPC, Big Data and Quantum Computing – PNRR Project, funded by the European Union – Next Generation EU. As concerns the ArtEmis Project, views and opinions expressed are however those of the author(s) only and do not necessarily reflect those of the European Union or European Commission-Euratom. Neither the European Union nor the granting authority can be held responsible for them.

AUTHOR DECLARATIONS

Conflict of Interest

The authors have no conflicts to disclose.

Author Contributions

Vincenzo Guerriero: Conceptualization (lead); Data curation (lead); Funding acquisition (supporting); Formal analysis (lead); Investigation (lead); Methodology (lead); Project administration (equal); Resources (equal); Software (lead); Supervision (lead); Validation (lead); Visualization (lead); Writing – original draft (lead). **Marco Tallini:** Data curation (supporting); Funding acquisition (lead); Investigation (supporting); Project administration (equal); Resources (equal); Supervision (supporting); Visualization (supporting).

DATA AVAILABILITY

The data that support the findings of this study are available from the corresponding author upon reasonable request.

APPENDIX A: MULTI-SCALE MLE EXOPNENT ESTIMATION

Equations (3)–(6) are derived from the observation that, given Eqs. (1) and (2) can be rewritten as

$$P(x) = \left(\frac{x}{x_{\min}}\right)^{-m}. \tag{A1}$$

Consequently, considering the normalized variable $z = x/x_{\min}$, two or more sub-populations (e.g., samples) gathered from the same population at different scales, with thresholds $x_{\min}1$, $x_{\min}2$,…, $x_{\min}k$,…, exhibit the same distribution $P(z) = z^{-m}$. The combined sample can be treated as a single data set with a total number of elements equal to the sum of the elements in the individual samples.

This consideration leads to a MLE formulation that is formally analogous to the one proposed by Navas-Portella *et al.*,[28] although there is a difference in the underlying assumptions. The formula by Ref. 28 applies to an aggregate of multiple statistical samples from different experiments, while in our case, the samples are drawn from the same population but at different scales. From this point on, the derivation of the formulations in Eqs. (3)–(6) is similar to that provided by Refs. 17 and 28. However, for completeness, we summarize it here, illustrating the proof of Eq. (3) as an example in the case of two samples with $N1$ and $N2$ elements and with thresholds $x_{\min}1$ and $x_{\min}2$.

For each sample, the probability density function $pdf(z)$ is given by the derivative of the distribution, $[1–P(z)]$,

$$pdf(z) = \frac{d}{dz}(1 - P(z)) = m \cdot z^{-(m+1)}. \tag{A2}$$

The likelihood function V (Refs. 17 and 31) is

$$\begin{aligned} V &= \prod_{j=1}^{N_1} (pdf(z_j)) \cdot \prod_{j=1}^{N_2} (pdf(z_j)) \\ &= \prod_{j=1}^{N_1+N_2} (m \cdot z_j{}^{-(m+1)}) = m^{N_1+N_2} \cdot \prod_{j=1}^{N_1+N_2} z_j{}^{-(m+1)}. \end{aligned} \tag{A3}$$

To find the value of the parameter m, which maximizes V, we set its derivative with respect to such parameter to zero. It is usually convenient to derive the log-likelihood,[17,31] here denoted by LV, i.e., the natural logarithm of the likelihood,

$$LV = (N_1 + N_2) \cdot \ln(m) + \sum_{j=1}^{N_1+N_2} (-(m+1) \cdot \ln(z_j)). \tag{A4}$$

Setting the derivative to zero yields

$$\frac{\partial}{\partial m} LV = (N_1 + N_2) \cdot \frac{1}{m} - \sum_{j=1}^{N_1+N_2} \ln(z_j) = 0, \tag{A5}$$

which leads to

$$m = \frac{N_1 + N_2}{\sum_{j=1}^{N_1+N_2} \ln(z_j)}. \tag{A6}$$

Recalling the definition of the variable z, it is clear that Eq. (6) is equivalent to Eq. (3).

The same procedure can be easily applied to the case of three or more samples, leading to Eq. (5). Based on the same considerations, Newman's expression[17] for the expected error can be extended to the case of two or more samples exhibiting a

TABLE I. Upper and lower limits of the 97.47% confidence interval for the Poisson random variable for number of occurrences ranging from 10 to 99.

Occurr.	Lower limit	Upper limit	Occurr.	Lower limit	Upper limit	Occurr.	Lower limit	Upper limit	Occurr.	Lower limit	Upper limit	Occurr.	Lower limit	Upper limit
10	4.936	19.72	28	18.30	42.37	46	33.00	63.67	64	48.30	84.37	82	63.95	104.7
11	5.606	21.05	29	19.09	43.57	47	33.84	64.83	65	49.16	85.51	83	64.83	105.8
12	6.289	22.37	30	19.89	44.78	48	34.68	65.99	66	50.02	86.65	84	65.71	107.0
13	6.984	23.67	31	20.69	45.98	49	35.52	67.15	67	50.89	87.78	85	66.59	108.1
14	7.689	24.97	32	21.49	47.17	50	36.36	68.31	68	51.75	88.92	86	67.47	109.2
15	8.404	26.26	33	22.30	48.37	51	37.21	69.46	69	52.62	90.05	87	68.35	110.3
16	9.128	27.53	34	23.11	49.56	52	38.05	70.62	70	53.48	91.19	88	69.23	111.4
17	9.860	28.80	35	23.92	50.75	53	38.90	71.77	71	54.35	92.32	89	70.11	112.6
18	10.60	30.06	36	24.74	51.93	54	39.75	72.92	72	55.22	93.45	90	70.99	113.7
19	11.35	31.32	37	25.55	53.12	55	40.60	74.07	73	56.09	94.58	91	71.87	114.8
20	12.10	32.57	38	26.37	54.30	56	41.45	75.22	74	56.96	95.71	92	72.76	115.9
21	12.86	33.81	39	27.19	55.48	57	42.30	76.37	75	57.83	96.84	93	73.64	117.0
22	13.62	35.05	40	28.02	56.65	58	43.15	77.52	76	58.70	97.97	94	74.53	118.1
23	14.39	36.28	41	28.84	57.83	59	44.01	78.66	77	59.58	99.10	95	75.41	119.3
24	15.16	37.50	42	29.67	59.00	60	44.86	79.81	78	60.45	100.2	96	76.30	120.4
25	15.94	38.73	43	30,50	60.17	61	45.72	80.95	79	61.32	101.3	97	77.18	121.5
26	16.72	39.94	44	31.33	61.34	62	46.58	82.09	80	62.20	102.5	98	78.07	122.6
27	17.51	41.16	45	32.17	62.50	63	47.44	83.23	81	63.08	103.6	99	78.96	123.7

power-law distribution with the same exponent, yielding Eqs. (4) and (6).

APPENDIX B: CONFIDENCE INTERVAL FOR THE POISSON RANDOM VARIABLE

Table I shows the 97.47% CI for the Poisson random variable. By way of example, we show the use of this table to estimate the CI of the measured frequency, in the above illustrated example of fracture analysis in rock. In the 19 mm long micro-scanline conducted over a thin section of rock, 24 joint aperture values greater than or equal to 0.005 mm were detected. This yielded a frequency (in fractures per meter) estimate $F1 = 24/0.019\,\mathrm{m} = 1260\,\mathrm{m}^{-1}$. The CI for $F1$ is estimated based on the CI of the number of occurrences, i.e., 24, assuming a Poisson spatial distribution for fractures. Based on the table above, the lower and upper limits of the 97.47% CI around the value of 24 are 15.16 and 37.50, respectively. Consequently, the lower and upper limits of the 97.47% CI for frequency are, respectively, $F_{\mathrm{low}}1 = 15.16/0.019\,\mathrm{m} = 798\,\mathrm{m}^{-1}$ and $F_{\mathrm{upp}}1 = 37.5/0.019\,\mathrm{m} = 1974\,\mathrm{m}^{-1}$. The same applies to frequency $F2$ measured on the outcrop scanline. The estimation of the two 97.47% CIs of $F1$ and $F2$ allows us to estimate the 95% CI of the TPF trendline slope m.

REFERENCES

[1]B. B. Mandelbrot and R. L. Hudson, *The (Mis)Behaviour of Markets—A Fractal View of Risk, Ruin and Reward* (Profile Books Ltd., 2008).
[2]L. A. Adamic and B. A. Huberman, "The Nature of Markets on the World Wide Web," *IEA5* (2000).
[3]S. B. Akhundjanov and L. Chamberlain, "The power-law distribution of agricultural land size," J. Appl. Stat. **46**(16), 3044–3056 (2019).
[4]B. Beare and A. K. Toda, "On the emergence of a power law in the distribution of COVID-19 cases," Physica D **412**, 132649 (2020).
[5]B. Blasius, "Power-law distribution in the number of confirmed COVID-19 cases," Chaos **30**(9), 093123 (2020).
[6]K. Zhao, M. Musolesi, P. Hui, W. Rao, and S. Tarkoma, "Explaining the power-law distribution of human mobility through transportation modality decomposition," Sci. Rep. **5**, 9136 (2015).
[7]N. Eikmeier and D. F. Gleich, "Revisiting power-law distributions in spectra of real world networks," in *Proceedings of the 23rd ACM SIGKDD International Conference on Knowledge Discovery and Data Mining (KDD'17)* (Association for Computing Machinery, New York, 2017), pp. 817–826.
[8]C. Petersen, J. G. Simonsen, and C. Lioma, "Power law distributions in information retrieval," ACM Trans. Inf. Syst. **34**(2), 1 (2016).
[9]M. A. M. Safari, M. Nurulkamal, I. Kamarulzaman, and A. D. Nasr Ahmed, "The power-law distribution for the income of poor households," Physica A **557**, 124893 (2020).
[10]Y. Honglin, C. Shou, Y. Yan, "Multiscale relationship analysis of power-law distribution and correlation in Chinese stock market," in *IEEE International Conference on Grey Systems and Intelligent Services* (IEEE, Nanjing, 2007), pp. 172–177.
[11]G. C. Crawford, H. Aguinis, B. Lichtenstein, P. Davidsson, and B. McKelvey, "Power law distributions in entrepreneurship: Implications for theory and research," J. Business Ventur. **30**(5), 696–713 (2015).
[12]Á. Corral and Á. González, "Power law size distributions in geoscience revisited," Earth Space Sci. **6**, 673–697 (2019).
[13]D. Sornette, *Critical Phenomena in Natural Sciences: Chaos, Fractals, Selforganization and Disorder. Concepts and Tools* (Springer, Berlin, 2000).
[14]D. L. Turcotte, "Self-organized criticality," Rep. Prog. Phys. **62**, 1377–1429 (1999).
[15]B. Mandelbrot, *The Fractal Geometry of Nature* (Freeman and Company, New York, 1983).
[16]A. Clauset, C. R. Shalizi, and M. E. J. Newman, "Power-law distributions in empirical data," SIAM Rev. **51**(4), 661–703 (2009).
[17]M. E. J. Newman, "Power laws, Pareto distributions and Zipf's law," Contemp. Phys. **46**(5), 323–351 (2005).
[18]O. J. Ortega, R. A. Marrett, and S. E. Laubach, "Scale-independent approach to fracture intensity and average spacing measurement," AAPG Bull. **90**, 193–208 (2006).
[19]M. Giorgioni, A. Iannace, M. D'Amore, F. Dati, L. Galluccio, V. Guerriero, S. Mazzoli, M. Parente, C. Strauss, and S. Vitale, "Impact of early dolomitization on multi-scale petrophysical heterogeneities and fracture intensity of low-porosity

platform carbonates (Albian-Cenomanian, southern Apennines, Italy)," Mar. Pet. Geol. **73**, 462–478 (2016).
[20]V. Guerriero, S. Vitale, S. Ciarcia, and S. Mazzoli, "Improved statistical multi-scale analysis of fractured reservoir analogues," Tectonophysics **504**(1–4), 14–24 (2011).
[21]V. Guerriero, S. Mazzoli, A. Iannace, S. Vitale, A. Carravetta, and C. Strauss, "A permeability model for naturally fractured carbonate reservoirs," Mar. Pet. Geol. **40**, 115–134 (2013).
[22]J. N. Hooker, S. E. Laubach, and R. Marrett, "A universal power-law scaling exponent for fracture apertures in sandstone," Geol. Soc. Am. Bull. **126**, 1340–1362 (2014).
[23]V. Guerriero and S. Mazzoli, "Theory of effective stress in soil and rock and implications for fracturing processes: A review," Geosciences **11**(3), 119 (2021).
[24]P. A. Gillespie, C. B. Howard, J. J. Walsh, and J. Watterson, "Measurement and characterisation of spatial distributions of fractures," Tectonophysics **226**(1, 4), 113–141 (1993).
[25]J. Baró and E. Vives, "Analysis of power-law exponents by maximum-likelihood maps," Phys. Rev. E **85**, 066121 (2012).
[26]H. Bauke, "Parameter estimation for power-law distributions by maximum likelihood methods," Eur. Phys. J. B **58**, 167–173 (2007).
[27]E. P. White, B. J. Enquist, and J. L. Green, "On estimating the exponent of power law distributions," Ecology **89**(4), 905–912 (2008).
[28]V. Navas-Portella, I. Serra, Á. Corral, and E. Vives, "Increasing power-law range in avalanche amplitude and energy distributions," Phys. Rev. E **97**, 022134 (2018).
[29]V. Navas-Portella, Á. González, I. Serra, E. Vives, and Á. Corral, "Universality of power-law exponents by means of maximum-likelihood estimation," Phys. Rev. E **100**, 062106 (2019).
[30]A. Deluca and Á. Corral, "Fitting and goodness-of-fit test of non-truncated and truncated power-law distributions," Acta Geophys. **61**, 1351–1394 (2013).
[31]F. M. Dekking, C. Kraaikamp, H. P. Lopuhaa, and L. E. Meester, *A Modern Introduction to Probability and Statistics: Understanding Why and How* (Springer-Verlag, 2005).
[32]L. Wasserman, *All of Statistics: A Concise Course in Statistical Inference* (Springer-Verlag, New York, 2004).
[33]M. P. Deisenroth, A. A. Faisal, and C. S. Ong, *Mathematics for Machine Learning* (Cambridge University Press, Cambridge, 2020).
[34]US National Research Council, *Review of Recommendations for Probabilistic Seismic Hazard Analysis: Guidance on Uncertainty and Use of Experts* (The National Academy Press, Washington, DC, 1997).
[35]P. Zamankhan, A. Mazouchi, and P. Sarkomaa, "Some qualitative features of the Couette flow of monodisperse, smooth, inelastic spherical particles," Appl. Phys. Lett. **71**(26), 3790–3792 (1997).
[36]P. Zamankhan, "Thermal measurements of boiling granular films," Rev. Sci. Instrum. **95**(5), 054902 (2024).